Electron capture collisions between Na$^+$ and O$_2$, N$_2$, and CO in the energy range 0.1–1 keV

R. Odom, D. Siedler, and J. Weiner

Department of Chemistry, Dartmouth College, Hanover, New Hampshire 03755

(Received 8 March 1976)

Absolute cross sections for charge transfer into several excited levels of sodium have been determined over the energy range 0.1–1 keV. The energy dependence of all cross sections appears to follow the form $\sigma(v, \Delta E) = Ke^{-\Delta E a / \hbar v}$, where v is the ion velocity and $\Delta E(n, l)$ is the "energy defect" for charge transfer into n, l excited levels of sodium. This experiment is the first test of the adiabatic hypothesis in which v and ΔE can be treated in the above expression essentially as independent variables. We find that at constant v, relative magnitudes of electron-capture cross sections are governed by the energy defect without regard to principal quantum number or angular momentum of the final state. This functional dependence is discussed in terms of a semiclassical coupled harmonic oscillator model.

I. INTRODUCTION

Charge transfer is a three-body rearrangement collision which has been the subject of intensive investigation, both experimental and theoretical, for over three decades.[1-6] Yet despite this prolonged effort, the nature of the process is well characterized only under special circumstances. Thus, general theory is tractable where nuclear and electronic motion may be effectively decoupled (at least in zeroth order). The two obvious cases are (i) the high-energy limit (Born approximation)[3,5,7] where collisional interaction time is short relative to the orbital period of the active electron and (ii) the low-energy limit[3,5,7] (adiabatic approximation) where the time of collision is long relative to the electron orbital period, and where nuclear motion may be incorporated parametrically into the system wave function. Even in the adiabatic regime the theory is clear-cut only for resonant charge exchange between identical ion cores.[8,9] Until recently, experimentalists confined their attention to high-energy (10–100 keV) collisions between simple atomic species such as protons, hydrogen, and helium.[5] In the past ten years, however, studies in the lower-energy regime have revealed dramatic quantum interference effects both in angular differential[10-12] and in total[13-17,23] cross-section measurements.

We report here the initial results of a long-term study into the nature of luminescent ion-molecule interactions. We observe sodium atomic photon emissions arising from charge transfer between Na$^+$ and O$_2$, CO, and N$_2$. Analysis of the observed emission rates in terms of cascade and electron-capture processes (Sec. III) leads us to a determination of absolute charge-transfer (CT) cross sections for several excited states of sodium. In Sec. V we discuss the functional dependence of charge transfer on collision energy, the n, l quantum numbers of the active electron, and the endoergicity or "energy defect" of the process.

It is our hope that results presented here will stimulate complementary theoretical development of charge-transfer processes in ion–diatomic-molecule collisions.

II. DESCRIPTION OF THE APPARATUS

The apparatus used to perform these experiments consists of an alkali-ion source, light-detection system, and ion-current collector housed in a cylindrical vacuum chamber. The basic experimental configuration is the following: A neutral target gas at low pressure is admitted to the vacuum chamber, and a beam of sodium ions of known energy passes through the gas and under the first lens of a light-detection system. Light emitted from the collision/reaction of the Na$^+$ ions with the target gas is focused on the entrance slit of a monochromator-photomultiplier tube (PMT) system. After passage below the light-detection system, the sodium-ion beam is collected on a Faraday cup. The photon count rate as a function of the ion-beam energy and intensity, wavelength, and target-gas density form the basis of the results presented here. Figure 1 shows a simplified schematic of the apparatus.

The vacuum chamber is a stainless-steel cylinder (25.4 cm diameter, 38.1 cm height) with eight vacuum ports mounted along its lower periphery. The chamber is pumped by a 6-in. LN$_2$-trapped oil diffusion pump. Auxiliary pumping is provided by a 4-in. pump connected to the main chamber through one of the ports. Other equipment mounted on the lower ports include the source assembly (described below), vacuum ionization gauge, gas inlet line, and a capacitance manometer. The reference side of this manometer is pumped by a 2-in. LN$_2$-trapped oil diffusion pump. The light de-
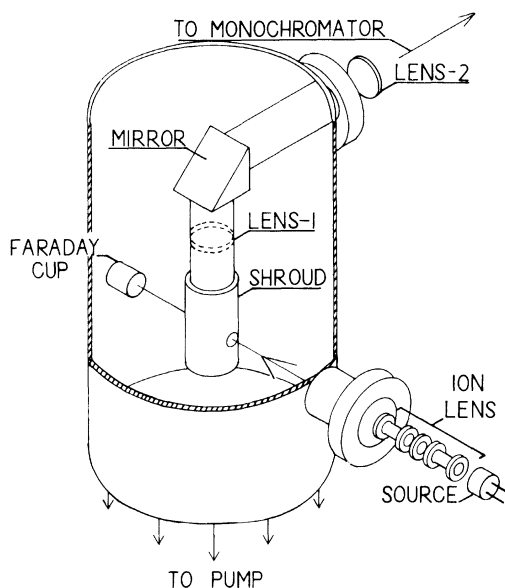
FIG. 1. Exploded schematic of the appartus. Inessential features such as vacuum ports, gas inlet, etc., are omitted. Actual position of Faraday cup is immediately behind scattered-light baffle (labeled "shroud").

tection system mounts in the chamber through a port located near the top of the cylinder, and the monochromator is attached directly to this vacuum flange. The Faraday cup is attached to a rotating mount (not pictured) which is supported from the top of the vacuum chamber. Background pressures of $\sim 10^{-6}$ Torr and operating pressures of $\sim 2 \times 10^{-4}$ Torr are typical.

The ion source used to produce the Na^+ beam consists essentially of a sodium salt embedded in a sintered tungsten wafer. The source is mounted on a stainless-steel housing, and the Na^+ beam is formed by resistive heating of the wafer. The energy of the beam is fixed by placing a positive potential on both the source and housing. After leaving the source, the beam is focused by an einzel lens, best focus corresponding to the maximum ion current collected on the cup. Ion beams ~ 0.5 μA with a heating power of 60 W are typical.

The light-detection system is a periscope type of arrangement used to bend the emitted light 90° and focus it on the entrance slit of a 0.25-m monochromator. As shown in Fig. 1, the 1-in.-diam. quartz lens $(f/1)$ located directly above the ion-beam path is held in a sleeve which attaches to the mirror mounting block. This lens focuses the light on the first surface mirror which is oriented at a 45° angle with respect to the normal of the plane of the first lens. Slots are cut into the sleeve in order that the optimum position of the first lens could be easily found. The light is reflected through 90° by a first surface mirror, passes through a col-

limating lens, and finally is focused by a third lens onto the monochromator entrance slit. This third lens also serves as the interface between the vacuum system and the laboratory, and is therefore mounted in a O-ring sealed holder.

Photons passing through the monochromator strike the cathode of a cooled RCA C31034 PMT. The voltage pulses from the tube are amplified, discriminated, and finally counted in 10-sec sampling intervals. Monochromator entrance and exit slits of 0.16 cm width were found to be the best compromise between intensity and resolution. Full width at half maximum (FWHM) of the triangular slit function is 6 nm for the 589.2-, 819.1-, and 498.1-nm lines of sodium, while the FWHM for the 330.2-nm line is 3.0 nm. The linewidth and shape were determined by substituting a sodium discharge lamp for the ion-beam signal in the interaction region.

III. DATA ACQUISITION, CROSS-SECTION EVALUATION, AND ERROR ANALYSIS

A. Data acquisition

For each of the observed excited sodium transitions, the photon count rate as a function of the sodium-ion energy was recorded. The signal count rate was the difference between 10-sec averages of the observed count rate with and without target gas in the chamber. For the strong transitions, e.g., $3p \to 3s$, we observed maximum signal count rates on the order of 1000 counts per second (cps), and for the weaker transitions, e.g., $5d \to 3p$, signal count rates on the order of 20 cps were typical with a "dark-count" rate of 2–3 cps. We also measured the dependence of the signal count rate on the target-gas pressure, and determined the instrumental line shape about the central wavelength of the sodium emission lines. The pressure-dependence studies showed that for each transition observed, the signal count rates extrapolated to zero at zero pressure, and were linear over the sampled pressure range $(0.1–5 \times 10^{-4}$ Torr). These results affirm that single-collision conditions prevailed at the target-gas pressure used $(\sim 2 \times 10^{-4}$ Torr) in this work. The line shape of the signal count rate about each transition wavelength was compared to known Na transition line shapes measured with a sodium-discharge lamp. We confirmed that the central peak and FWHM were identical for each case. In addition, we investigated the polarization of the emitted light using a polarizer and interference filters in place of the monochromator. The results of this investigation showed that for the Na $3p \to 3s$ transition the emitted light was not preferentially polarized parallel or perpendicular to the ion-beam axis in any system discussed here.

B. Cross-section evaluation

The rate equation governing the population of a particular quantum state j of the sodium atom is given by

$$v\frac{dn_j(z)}{dz} = \frac{i(z)}{q} N_B\sigma_{CT}(j) + \sum_{k>j} \frac{n_k(z)}{\tau_{k\to j}} - \frac{n_j(z)}{T_j}, \quad (3.1)$$

where $n_j(z)$ and $n_k(z)$ are the populations per unit length along the beam of states j and k, respectively; v and $i(z)/q$ are the velocity and particle flux of the sodium-ion beam, N_B is the target-gas density, $\sigma_{CT}(j)$ is the charge-transfer cross section into the jth state, $\tau_{k\to j}$ is the mean lifetime of the kth state for transition into the jth state, and T_j is the net lifetime against all possible decay channels of the jth state. The first two terms on the right of Eq. (3.1) are the populating contributions due to charge transfer and k- to j- state cascading, respectively, while the final term represents all the depopulating channels of the j state. In order to evaluate the charge-transfer cross sections, it is necessary to calculate from Eq. (3.1) the mean emission rate for each state and equate this to the experimentally observed emission rate. The mean emission rate is simply the population of the state along the effective length of the beam divided by the lifetime for the transition observed. We calculate the charge-transfer cross section $\sigma_{CT}(j)$ from the relation

$$\int_0^{z_0} \frac{n_j(z)\,dz}{\tau_{j\to i}} = \frac{\langle S(\lambda)\rangle_{obs}}{I(\lambda)}. \quad (3.2)$$

Thus, one must initially solve Eq. (3.1) for $n_j(z)$ and then integrate the result from zero to z_0 in Eq. (3.2). In the above expression, z_0 is the effective length of the ion beam and in this work is 10.8 cm; $\langle S(\lambda)\rangle_{obs}$ is the observed average signal count rate at wavelength λ corresponding to the $j\to i$ transition; and $I(\lambda)$ is the efficiency of the optical detection system at λ. This efficiency is discussed in detail in Sec. IV.

For the cross sections reported here, two assumptions were made in the solution of Eq. (3.1). The first assumption is that the ion current $i(z)$ is constant over the effective length of the beam. This assumption is valid since only a 5% attenuation of the ion beam is observed at the target-gas pressure used. The second assumption is that the uppermost states in Eq. (3.1) are formed only by direct charge transfer; i.e., the k-state populations are governed by the following rate equation:

$$v\frac{dn_k(z)}{dz} = \frac{i}{q} N_B\sigma_{CT}(k) - \frac{n_k(z)}{T_k}, \quad (3.3)$$

and therefore

$$n_k(z) = \frac{iN_B}{q}\sigma_{CT}(k) T_k\left[1 - \exp\left(-\frac{z}{vT_k}\right)\right]. \quad (3.4)$$

Using this expression for $n_k(z)$ in Eq. (1) leads to the following expression for the mean emission rate from state j to state i:

$$\frac{N_j}{\tau_{j\to i}}(z_0) = \frac{\int_0^{z_0} n_j(z)\,dz}{\tau_{j\to i}} = \frac{iN_B}{q\tau_{j\to i}}\left(\sigma_{CT}(j)f(z_0,v,T_j)T_j + \sum_{k>j}\frac{\sigma_{CT}(k)T_kT_j}{\tau_{k\to j}(T_k-T_j)}\left[T_kf(z_0,v,T_k) - T_jf(z_0,v,T_j)\right]\right),$$

$$(3.5)$$

and solving this expression for $\sigma_{CT}(j)$ gives

$$\sigma_{CT}(j) = \frac{q\tau_{j\to i}}{iN_BT_jf(z_0,v,T_j)}\left(\frac{N_j(z_0)}{\tau_{j\to i}} - \frac{iN_BT_j}{q\tau_{j\to i}}\sum_{k>j}\frac{\sigma_{CT}(k)T_k}{\tau_{k\to j}(T_k-T_j)}[T_kf(z_0,v,T_k) - T_jf(z_0,v,T_j)]\right) \quad (3.6)$$

where

$$f(z_0,v,T_j) = z_0\{1 - vT_j[1 - \exp(-z_0/vT_j)]\}.$$

The charge-transfer cross sections into the k states are obtained by integrating Eq. (3.4) over the effective length and using Eq. (3.2) for each transition studied. The various lifetimes of the excited states are known and tabulated.[18] Therefore, under the assumptions stated above, the capture cross sections into the various j states can be calculated from Eq. (3.6).

It is now necessary to consider the possible pop-

ulating and depopulating channels existing for the excited sodium levels we have observed in this work. Figure 2 is a diagram illustrating the population of some of the lower-lying levels via the electron capture process. This figure also shows the possible transitions between levels. Table I is a list of the observed sodium excitations produced from the electron capture process, and this table also gives the important populating and depopulating transitions for each level.

Considering first the ns states, we obtained no information concerning the capture cross sections into the 3s or 4s states. The 3s state is, of course,
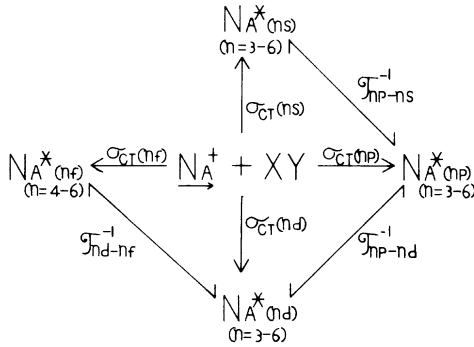
FIG. 2. Schematic flow diagram of competing gain-loss processes included in calculation of charge-transfer cross sections from observed emission rates.

the ground state, and the wavelength of the $4s \to 3p$ transition (1140 nm) is too far into the infrared to be detected. The $5s$ state was treated as being populated only by electron capture since the $np \to 5s$ ($n > 5$) transition lifetimes are not available. The cross section for formation of the $5s$ state is evaluated directly only for the (Na^+, N_2) system because it was impossible to estimate the contribution of the strong O* transition at 615.7 nm to the count rates for the O_2 or CO systems. The cross sections for capture into the $6s$ state are not reported because the observed signal count rates for the $6s \to 3p$ transition are small (~ 4 cps) and the resultant uncertainties are high ($\pm$ 100%).

Turning next to the np levels, we considered the $5p$ and $6p$ levels as being formed only by electron capture because the transition probabilities for the $nd \to 5p$ ($n = 5-7$), $ns \to 5p$ ($n = 6, 7$), and $6d, 6s, 7d$

TABLE I. List of populating-depopulating channels for the observed sodium states.

State	Transition observed	λ (nm)	Populating channels	Depopulating channels
$5s$	$5s \to 3p$ (N_2)	615.9	CT	$5s \to 3p, 4p$
$3p$	$3p \to 3s$	589.2	CT, $nd \to 3p$ ($n = 3-6$) $ns \to 3p$ ($n = 4-6$)	$3p \to 3s$
$4p$	$4p \to 3s$	330.2	CT, $nd \to 4p$ ($n = 4-6$) $6, 7s \to 4p$	$4p \to 3d, 3s, 4s$
$5p$	$5p \to 3s$	285.3	CT	$5p \to 3s, 4s$
$6p$	$6p \to 3s$ (O_2)	268.0	CT	$6p \to 3s, 4s$
$3d$	$3d \to 3p$	819.1	CT, $nf \to 3d$ ($n = 4-6$)	$3d \to 3p$
$4d$	$4d \to 3p$	568.6	CT	$4d \to 3p, 4p$
$5d$	$5d \to 3p$	498.1	CT	$5d \to 3p, 4p$

$\to 6p$ are not tabulated. In addition, if we use the $6s, 6d \to 5p$ transition probabilities for the hydrogen atom and estimate the charge-transfer cross sections into these two levels, we find that the $5p$ cross section decreases by less than 1%. The possible depopulating channels for these two levels are the transitions into the $4s$ and $3s$ states; the $5p, 6p$ $\to 3s$ transitions were observed. The populating channels for the $4p$ levels include the transitions $nd \to 4p$ ($n = 4-6$) and $6, 7s \to 4p$. These latter two transitions were ignored since the capture cross sections into these levels were observed to be very small. The output channels for the $4p$ level are the $4p \to 3s, 3d$, and $4s$ transitions. The $3p$ level has the the largest number of populating channels; included among these are the $nd \to 3p$ ($n = 3-6$) and $ns \to 3p$ ($n = 4, 5$) transitions. The contribution to the $3p$ population from the $nd \to 3p$ transitions can be evaluated from the nd capture cross-section data which are discussed in detail below. The $ns \to 3p$ contribution cannot be directly evaluated since, except for the $5s$ state from the (Na^+, N_2) system, we have no cross-section data for the $4s$ or $5s$ states (see above). In order to estimate this contribution, we have adopted the following procedure: As is discussed in Sec. V, the logarithm of the capture cross section is directly proportional to the energy defect ΔE. Therefore, for each target gas, an estimate of the $4s$ and $5s$ capture cross sections can be made from the $\ln \sigma_{CT}$ vs ΔE plots (see Fig. 8). We use these estimates as additional $\sigma_{CT}(k)$ terms in Eq. (3.6) and compare the $3p$ cross sections calculated with and without these additional channels. For example, for the (Na^+, O_2) system at 1000 eV, the $\sigma_{CT}(4s)$ and $\sigma_{CT}(5s)$ are found to be 0.8×10^{-19} and 0.06×10^{-19} cm^2, respectively. Using these values in Eq. (3.6), it is found that the $3p$ cross section for *direct* charge transfer decreases by 10%.

Finally, for the nd levels, we have assumed that the 4 and $5d$ levels are populated only by electron capture. The output channels for these levels are the $4, 5d \to 3p, 4p$ transitions. The procedure for estimating the contribution to $3p, 4p$ populations from these transitions is the same as described above for the $ns \to 3p$ transitions. In the case of the $3d$ level, the transition probabilities $4, 5, 6f \to 3d$ are tabulated,[18] so that by estimating $\sigma_{CT}(4, 5, 6f)$ via Fig. 8 we calculate the f-level cascade contributions to $3d$. Estimated cross-section values at 1000 eV for the (Na^+, O_2) system are $\sigma_{CT}(4f) = 0.38$ $\times 10^{-20}$, $\sigma_{CT}(5f) = 0.14 \times 10^{-20}$, and $\sigma_{CT}(6f) = 0.10$ $\times 10^{-20}$ cm^2. For this system, the calculated $3d$ charge-transfer cross section decreases by 4% when the input cascade channels ($nf \to 3d$) are considered. The $3d \to 3p$ transition is the only depopulating channel for this level.

C. Error analysis

Total emission (TE) cross sections, from which we calculate charge-transfer cross sections (see Sec. II B), are directly related to experimental measurements via

$$\sigma_{TE} = \frac{\langle S(\lambda) \rangle}{(i/q) N l I(\lambda)}, \qquad (3.7)$$

where $\langle S(\lambda) \rangle$ is the average signal count rate, $\epsilon(\lambda)$ the optical detection efficiency, i/q the ion particle flux, N the number density of target gas, l the effective length of beam path over which photons are detected (determined empirically and assumed to be known exactly), and σ_{TE} the cross section for total emission. From elementary random-error analysis,

$$\frac{\delta \sigma_{TE}}{\sigma_{TE}} = \left[\left(\frac{\delta \langle S(\lambda) \rangle}{\langle S(\lambda) \rangle} \right)^2 + \left(\frac{\delta I(\lambda)}{I(\lambda)} \right)^2 + \left(\frac{\delta i}{q} \right)^2 + \left(\frac{\delta N}{N} \right)^2 \right]^{1/2},$$
$$(3.8)$$

where $\delta(x)$ denotes uncertainty in the measurement of x. Variations in ion-beam current and neutral-gas pressure are negligible during an experimental run. Therefore we take $\delta i/q$ and $\delta N/N$ to be the specified accuracies of the measuring instruments themselves (5% and 2%, respectively). Random error in the optical detection efficiency, $\delta I(\lambda)/I(\lambda)$, is estimated from several independent calibration experiments. We find a reproducibility of about 15%. Finally, we calculate $\delta \langle S(\lambda) \rangle / \langle S(\lambda) \rangle$ assuming Poisson statistics in the photon count rate. Here the uncertainties range from 3% to 22%, depending on signal intensity. Use of Eq. (3.8), therefore, leads to an overall random error in the cross section ranging from 15% to 27%.

Although we have taken pains to exclude systematic error from the optical calibration, a possibility still exists that the *absolute* cross sections may be well outside the random-error limits. Only several independent checks from different laboratories on the same system can give real confidence in establishing absolute values. However, we find that run-to-run reproducibility is somewhat better than the error estimate calculated from Eq. (3.8) so that the energy dependence of *relative* cross sections (both *intra-* and *intersystem*) are reliable to to within about 10%.

IV. CALIBRATION OF THE OPTICAL SYSTEM

Our aim was to design a calibration scheme that would minimize the differences between experimental conditions during an actual measurement and a calibration run. Figure 3 is a schematic of the setup used to measure the absolute efficiency of the system. A standard lamp (tungsten-halogen)
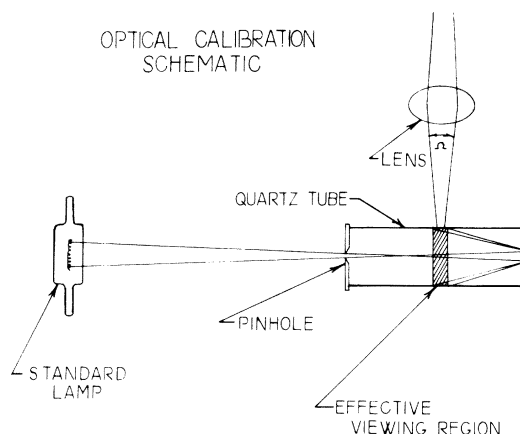
FIG. 3. Optical calibration scheme used in absolute cross-section determinations. Quartz tube is frosted to diffuse light. Effective viewing region is empirically determined in a separate experiment. Precision pinhole of 25 μm diameter is positioned about 60 cm from the standard lamp. A freshly prepared diffuse MgO coating is used to reflect incoming light off the back of the quartz tube.

calibrated in spectral irradiance to within 2% of NBS primary standards is positioned on the ion-beam axis a known distance (~60 cm) from the input aperture of the effective viewing region beneath the primary optical lens. The lamp is powered with regulated dc current monitored by the voltage drop across a precision (0.04%) shunt resistor in series with the light source. The calibrated photon flux entering the 25-μm precision pinhole illuminates a frosted quartz tube placed along the beam axis so as to simulate the geometry and intensity of light emission from the ion beam during an experiment. To insure uniform illumination, the entering photon flux is reflected from a diffuse magnesium-oxide-coated back plate as shown in the schematic. The effective viewing length of the primary lens (3.2 mm) was determined empirically in a separate experiment by moving a light source along the beam axis while measuring the response of the photomultiplier tube. The efficiency of the optical system is defined as the ratio of output count rate to input photon rate,

$$I(\lambda) = \gamma_{out} / \gamma_{in} .$$

The output count rate γ_{out} is determined with a high high-speed preamplifier-descriminator-counter combination, while γ_{in} is calculated by

$$\gamma_{in} = A(\lambda) A \Delta\lambda f,$$

where $A(\lambda)$ is the spectral irradiance of the standard lamp (photons sec^{-1} cm^{-2} nm^{-1}), A the area of the precision pinhole aperture (cm^2), $\Delta\lambda$ the bandpass of the monochromator (nm), and f the effective fractional solid angle subtended by the primary

lens of the optical system ($\Omega/4\pi$ in Fig. 3).

The efficiency I was determined directly at 590 nm. Efficiencies at other wavelengths were calculated by taking into account variations in phototube quantum efficiency and monochromator grating efficiency:

$$I(\lambda) = I(590)\frac{I_Q(\lambda)}{I_Q(590)}\frac{I_G(\lambda)}{I_G(590)}, \qquad (4.1)$$

where I_Q is the quantum efficiency and I_G the grating efficiency. Attempts were made to measure directly the system optical efficiency over the entire spectral range, but spurious photon counts due to scattered long-wavelength light in the monochromator did not permit direct determination in the near uv. Only over a relatively narrow band (450–600 nm) in the visible was direct determination possible. Within this band, however, $I(\lambda)$ calculated according to Eq. (4.1) is in good agreement with directly measured efficiencies. This agreement gives credence to our use of Eq. (4.1) as transfer function for calibration in the near-uv and ir spectral regions.

The optical calibration setup was dismantled and remounted several times over a two month period with a reproducibility of about 15%.

V. DISCUSSION

Two principal findings emerge from the study of these systems: electron capture cross sections *increase* exponentially with collision velocity and *decrease* exponentially with energy defect. These results are summarized in Figs. 4–8. We use the term "energy defect" with its customary meaning; it is simply the internal energy difference between initial and final states of the system at infinite nuclear separation.

The functional relation can be written

$$\sigma(v, \Delta E) \simeq Ke^{-\alpha\Delta E/v\hbar}, \qquad (5.1)$$

where v and ΔE are the relative collision velocity and energy defect, respectively, and α is a "characteristic length" of the collision event. This exponential behavior of the cross section in the adiabatic region has also been observed by Hasted.[19] The argument of the exponential in Eq. (1) is closely related to the celebrated Massey "adiabatic hypothesis," which states that the maximum probability of charge or energy transfer should occur when

$$\Delta E\alpha/v\hbar \simeq 1. \qquad (5.2)$$

As is well known, the Massey criterion is based on the simple semiclassical notion that the collision time $\tau \simeq \alpha/v$ must be close to the characteristic oscillatory period of the time-dependent non-
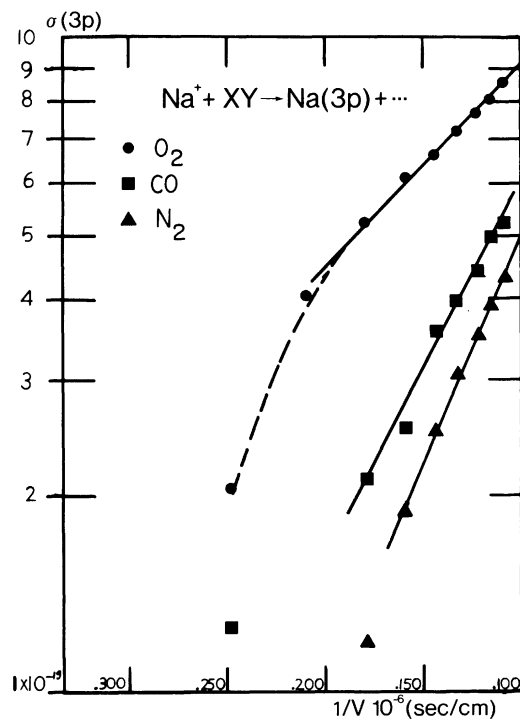
FIG. 4. Plots of σ_{CT} vs reciprocal of ion velocity for the $3p$ sodium transition. Linearity is evident. Deviation at low v may be due either to poor counting statistics or failure to substitute an "effective" collision velocity for the ion-beam velocity.
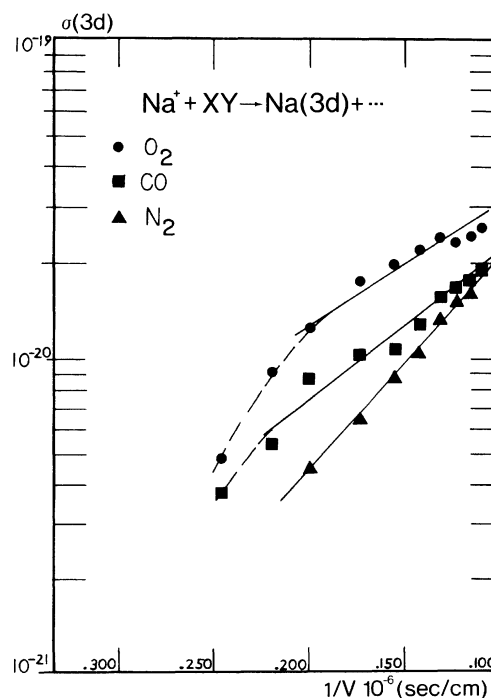
FIG. 5. Same as Fig. 4 except for the $3d$ transition.
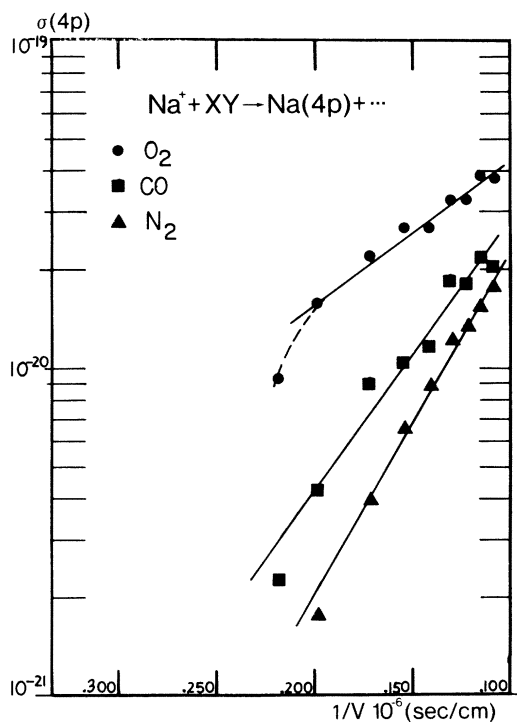
FIG. 6. Same as Fig. 4 except for the $4p$ transition.

stationary state of the collision intermediate. It is an elementary result of time-dependent first-order perturbation theory that this characteristic angular frequency is given by $w = \Delta E/\hbar$, where E is the en-
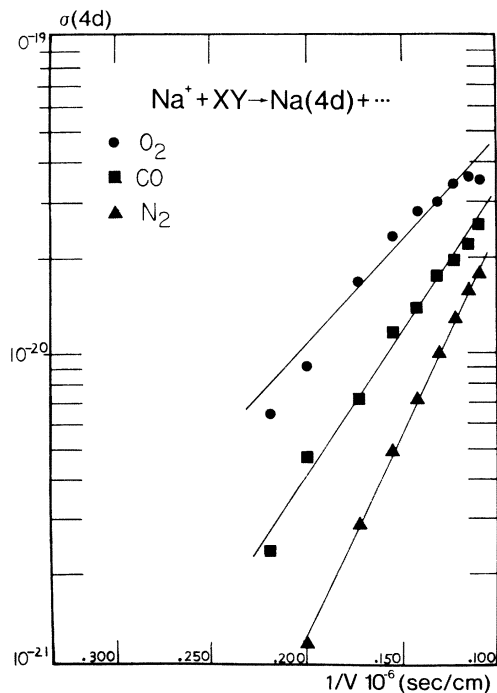
FIG. 7. Same as Fig. 4 except for the $4d$ transition.
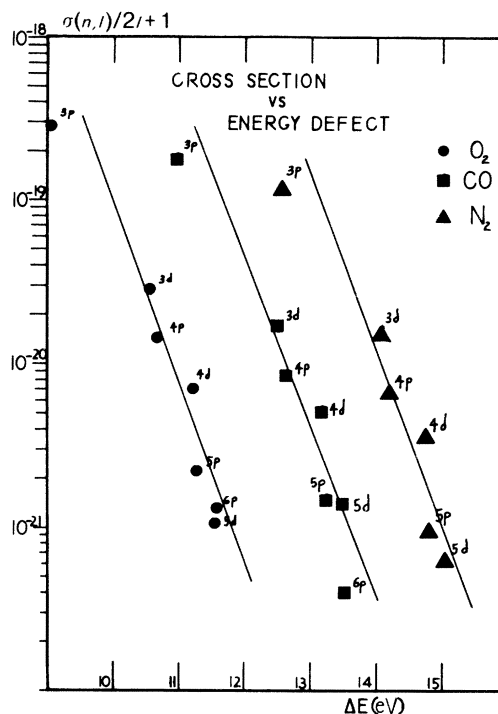
FIG. 8. Plot of $\log \sigma_{CT}$ vs energy defect ΔE for three systems studied. Note that cross sections have been normalized by the statistical weights of their appropriate atomic levels.

ergy difference between the coupled states. Although the Massey criterion has proved a useful benchmark against which experimental results from many diverse studies can be compared, it specifies (roughly) only the condition for maximum probability and implies nothing about the functional behavior of the cross section on either side of the peak. What is required is a fully developed quantum-mechanical treatment of a three-body rearrangement collision (charge transfer) between an atom and a diatom with large energy defect in the "adiabatic" collision-energy regime. We are aware of no such theory, although some recent work in the high-energy regime, i.e., where the relative collision velocity is sufficiently fast that the Born approximation can be invoked, appears to hold promise for the future.[20]

In lieu of an adequate theoretical treatment, therefore, we offer a crude model of the charge-transfer process which follows in the spirit of Massey's original discussion. We consider the dynamics of the active electron in a charge-transfer collision,

$$A^+ + (B^+ + e) \to [A^+ \cdots e \cdots B^+] \to (A^+ + e) + B^+,$$
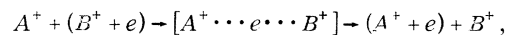
to be essentially that of a harmonically bound charge excited by the field of an ion moving in a
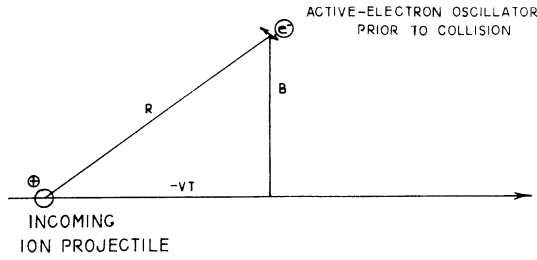
FIG. 9. Kinematic set-up for classical oscillator excitation by a moving point charge. Note that active electron is located at point P.

rectilinear orbit past the target with velocity v and impact parameter B. The kinematic picture is shown in Fig. 9. Near the distance of closest approach, the active electron begins to experience coupling to the A^+ ion. In the collision intermediate the electron oscillates back and forth between the A^+ and B^+ cores with a frequency w_0 equal to the difference between the simple harmonic frequencies associated with the states $(A^+ + e)$ and $(B^+ + e)$. Finally we consider the probability of electron capture to be proportional to the energy transferred to the active electron in the collision, ϵ. That is,

$$P_{b \to a} = K \epsilon(w_0).$$

It is important to emphasize that the perturbation on the active electron is a time-dependent force (Coulomb electric field) whose Fourier amplitude at w_0 essentially determines the degree of coupling. When the "time of collision" is such that w_0 is the principal contributor to the Fourier spectrum, then the energy transfer $\epsilon(w_0)$ and hence the probability of charge-transfer excitation will be a maximum. This remark is nothing more than a restatement of the Massey criterion. Owing to the large energy defects and low collision energies which obtain in the present studies, however, the Fourier amplitude of the perturbation at w_0 is so small that we can seek a limiting expression for $\epsilon(w_0)$. In order to calculate ϵ we turn to classical electrodynamics. Using the notation of Fig. 9, we see that a charged particle will produce two electric field components, parallel and perpendicular to its trajectory, at point P, the coordinate of the harmonically bound active electron. We assume of course that the spatial amplitude of the harmonic motion is small compared to the distance of closest approach, B.

These electric fields are given by

$$E_1 = eB/(B^2 + v^2 t^2)^{3/2},   (5.3)$$

$$E_2 = evt/(B^2 + v^2 t^2)^{3/2}.   (5.4)$$

It can be shown as a general result[21] that the ener-

gy transferred to an oscillator by an external electromagnetic field is given by

$$\epsilon = (\pi q^2/m)|E(w_0)|^2,   (5.5)$$

where q and m are the charge and mass of the oscillating charged particle, respectively, and $E(w_0)$ is the Fourier transform of the electric field evaluated at the characteristic frequency of the oscillation, w_0. In the charge-transfer situation we identify w_0 with the frequency of the coupled oscillators, $w_0 = |w_A - w_B|$.

Now from Eq. (5.3),

$$E_1(w) = \frac{eB}{(2\pi)^{1/2}} \int_{-\infty}^{+\infty} \frac{e^{iwt}}{(B^2 + v^2 t^2)^{3/2}} dt,$$

substituting $x = vt/B$, then

$$E_1(w) = \frac{e}{(2\pi)^{1/2} Bv} \int_{-\infty}^{+\infty} \frac{e^{iwBx/v}}{(1 + x^2)^{3/2}} dx$$

$$= \frac{e}{Bv} \left(\frac{2}{\pi}\right)^{1/2} \left[\frac{wB}{v} K_1\left(\frac{wB}{v}\right)\right],   (5.6)$$

$$E_2(w) = \frac{e}{(2\pi Bv)^{1/2}} \int_{-\infty}^{+\infty} \frac{e^{iwBx/v} x \, dx}{(1 + x^2)^{3/2}}$$

$$= \frac{-ie}{Bv} \left(\frac{2}{\pi}\right)^{1/2} \left[\frac{wB}{v} K_0\left(\frac{wB}{v}\right)\right],   (5.7)$$

where $K_1(wB/v)$ and $K_0(wB/v)$ are modified Bessel functions.

Letting $\beta = wB/v$ and substituting (5.6) and (5.7) into (5.5), we find

$$\epsilon = \frac{2e^4}{m_e v^2 B^2} \{\beta_0^2 [K_1^2(\beta_0) + K_0^2(\beta_0)]\}.$$

For $\beta \gg 1$, the asymptotic form of the modified Bessel functions is[22] $K_\nu(\beta) \to (\pi/2\beta)^{1/2} e^{-\beta}$ so that finally in the region of low velocity and high frequency $(\beta \gg 1)$ we find

$$\epsilon = \frac{2\pi}{m_e} \left(\frac{e^2}{vB} \beta_0^{1/2} e^{-\beta_0}\right)^2.   (5.8)$$

Equation (5.8) is the limiting expression for electron excitation which we have sought.

Now we note that the interaction energy at the distance of closest approach is

$$\epsilon_0 = e^2/B,$$

and letting $2B \simeq \alpha$ in Eq. (5.8), and $w_0 = \Delta E/\hbar$, we have

$$P_{b \to a} \propto \epsilon_0 \left(\frac{2\pi e^2 \Delta E}{m_e \hbar}\right) \frac{1}{v^3} e^{-\Delta E \alpha/\hbar v}.$$

(5.9)

Equation (5.9) is the basic result of the model. Assuming that electron transfer occurs over a
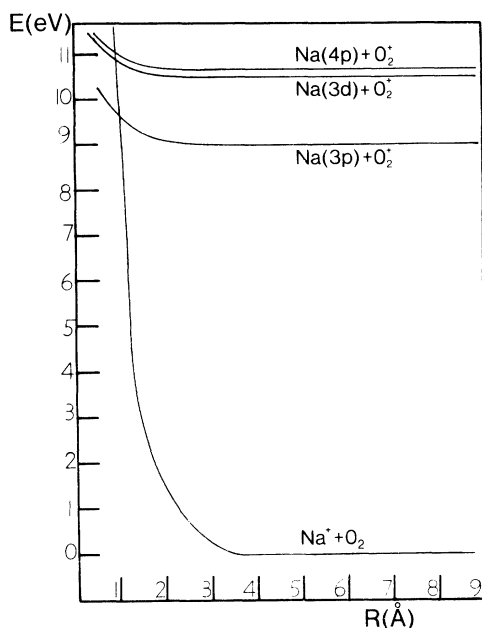
FIG. 10. A strictly schematic sketch of crude poten-
tial-energy surfaces common to most alkali-ion charge-
transfer situations. True positions of upper-state
crossings are unknown. Relative flatness and parallel
upturn at small internuclear distance is not an unrea-
sonable expectation for excited states. Plot shows that
use of energy defect at infinite nuclear separation is
obviously inadequate for quantitative calculation of
charge-transfer probability.

narrow range of impact parameter, we write

$$\sigma_{b \to a} = 2\pi \int_0^\infty P(B) B \, dB \simeq P(B_0)\pi B_0^2 ,$$

so that finally

$$\sigma_{b \to a}(v, \Delta E) = K(v)e^{-\Delta E \alpha / \hbar v}, \qquad (5.10)$$

and the observed functional dependence of the
cross section is proportional to the probability of
charge exchange.

Comparing Eq. (5.9) with Eq. (5.1), we see that
the classical electrodynamic model yields the ob-
served expenential dependence with a v^{-3} term in
the preexponential factor. Therefore, a plot of

lnσ vs $1/v$ should exhibit a straight line with slope
$-\Delta E\alpha/\hbar$ and an "intercept" $K(v)$ which is weakly
dependent on collision velocity. Over the energy
range 0.1–1 keV, ln$K(v)$ varies by only 8%. The
linearity of measured data, presented in lnσ-vs-$1/v$
plots, is evident in Figs. 4–8.

Two final remarks regarding the appropriateness
of this model are in order. First, we note that the
energy defects for all three systems are large,
and the electron-capture processes endoergic.
Therefore, no quantum interference effects are
expected from outer-branch potential surface
crossings or near-crossings. Indeed, we have ob-
served no quantum effects of any kind including
polarization of emission. This finding is in con-
trast to the recent work of Tolk et al.[14-17,23] where
interference effects from curve-crossing phenom-
ena dramatically influence behavior of the total
electron-capture cross section. Second, the mod-
el is clearly inadequate for quantitative calcula-
tions. The magnitude of the probability determined
by Eq. (5.9) is extremely sensitive to the value of
ΔE, and the use of ΔE at infinite internuclear distance
leads to charge-transfer probabilities unrealistically
small. It is equally clear that the actual electron-
transfer process takes place in these systems on
the steeply rising inner branches of the potential-
energy surfaces where differences between sur-
faces are certainly less than at infinite separation.
Figure 10 illustrates the point.

Although the essentially classical model present-
ed here can serve only to rationalize experimental
results, we hope it may serve the heuristic pur-
pose of stimulating a serious theoretical treatment
of ion-diatomic charge-transfer processes in the
adiabatic regime.

[1]H. S. W. Massey, Rep. Prog. Phys. 12, 248 (1948).
[2]*Atomic and Molecular Processes,* edited by D. R. Bates
(Academic, New York, 1962), Chaps. 14 and 18.
[3]N. F. Mott and H. S. W. Massey, *The Theory of Atomic
Collisions,* 3rd ed. (Oxford U.P., London, 1965).
[4]R. F. Stebbings, Adv. Chem. Phys. 10, 195 (1966).
[5]R. A. Mapleton, *Theory of Charge Exchange* (Wiley,
New York, 1972).
[6]E. W. Thomas, *Excitation in Heavy Particle Collisions*
(Wiley, New York, 1972).

[7]D. R. Bates and R. McCarroll, Adv. Phys. 11, 39 (1962).
[8]D. Rapp and W. E. Francis, J. Chem. Phys. 37, 2631
(1962).
[9]E. F. Gurnee and J. L. Magee, J. Chem. Phys. 26, 1237
(1952).
[10]F. P. Ziemba, G. J. Lockwood, G. H. Morgan, and
E. Everhart, Phys. Rev. 118, 1552 (1960).
[11]W. Lichten, Phys. Rev. 131, 229 (1963).
[12]W. Lichten, Phys. Rev. 139, A27 (1965).
[13]J. Perel, Phys. Rev. A 1, 369 (1970).

[14]N. H. Tolk, C. W. White, A. H. Dworetsky, and L. A. Farrow, Phys. Rev. Lett. 25, 1251 (1970).

[15]N. H. Tolk, C. W. White, A. H. Neff, and W. Lichten, Phys. Rev. Lett. 31, 671 (1973).

[16]T. Andersen, A. Nielsen, and K. T. Olsen, Phys. Rev. Lett. 31, 739 (1973).

[17]N. H. Tolk, J. C. Tully, C. W. White, J. Krauss, A. A. Monge, and A. H. Neff, Phys. Rev. Lett. 35, 1175 (1975).

[18]W. L. Wiese, M. W. Smith, and B. M. Miles, *Atomic Transition Probabilities* , NSRDS–NBS 22 (U.S. GPO, Washington, D. C., 1969), p. 1.

[19]J. B. Hasted, J. Appl. Phys. 30, 25 (1959).

[20]Y. B. Band, J. Phys. B 7, 2055 (1974).

[21]J. D. Jackson, *Classical Electrodynamics* (Wiley. New York, 1962), Chap. 13.

[22]M. Abramowitz, and S. A. Stegun, *Handbook of Mathe- matical Functions,* NBS Applied Math Series 55 (U.S. GPO, Washington, D.C., 1964), pp. 377 and 378.

[23]N. H. Tolk, J. C. Tully, C. W. White, J. Kraus, A. A. Monge, D. L. Simms, M. F. Robbins, A. H. Neff, and W. Lichten, Phys. Rev. A 13, 969 (1976).